*J. Fluid Mech.* (2000), *vol.* 404, *pp.* 251–268. Printed in the United Kingdom



# Do longshore bars shelter the shore?

By JIE YU AND CHIANG C. MEI

Department of Civil & Environmental Engineering, Massachusetts Institute of Technology, Cambridge, MA 02129, USA

(Received 28 May 1999 and in revised form 4 October 1999)

In most past theories on Bragg reflection of waves by a finite patch of *rigid* bars, only outgoing waves are allowed on the transmission side, simulating the effect of an idealized shoreline where all the incident wave energy is consumed by breaking. In these theories the amplitudes of both the incident and reflected waves are found to decrease monotonically over the bar patch in the shoreward direction. This result has motivated the idea of artificially constructing bars to protect a beach from incident waves. However, some numerical calculations have suggested that this tendency does not always hold when there is some reflection from the shore. We show here that with finite reflection by the shoreline the spatial distribution of wave energy over the patch can indeed be reversed, indicating that the mechanism can increase the hazards to the beach. The phase relation between the bars and the shoreline reflection is found to be the key to this qualitative change of wave response.

## 1. Introduction

When waves pass over a seabed covered with bars spaced at half of the water wavelength, reflection is amplified. This mechanism, called Bragg resonance in crystallography, is due to the constructive interference of reflected waves from successive bar crests. Since the experimental demonstration by Heathershaw (1982), this subject has been studied extensively by many researchers (Davies & Heathershaw 1984; Mei 1985; Kirby 1986, 1989, 1993; Dalrymple & Kirby 1986; Hara & Mei 1987; Liu 1987; Yoon & Liu 1987; Mei, Hara & Naciri 1988; Guazzelli, Rey & Belzons 1992; Rey, Guazzelli & Mei 1996; Mattioli 1990, 1991; Nayfeh & Hawwa 1994; etc. see Mei & Liu 1993 for a review). A common example treated in those studies is the scattering of waves by a finite patch of rigid bars on an otherwise plane bed; reflection from the beach toward the patch is assumed to be negligible. It is found that, when the incident wave and the bars are closely matched, the amplitudes of the incident and the reflected waves decrease monotonically toward the shore, suggesting that a bar patch sufficiently tuned to the incident waves can serve as a breakwater for protecting the shoreline (e.g. Mei *et al.* 1988; Baillard *et al.* 1990; Baillard, DeVries & Kirby 1992).

In nature, there is always some reflection from the shore, either because dissipation by breaking at the shore is incomplete or the beach slope is steep. With finite reflection from the shoreline, wave evolution over the bars can be more complicated. Some indication of this complexity was noted by Kirby & Anton (1990) in a numerical study. They considered a vertical wall at some distance downwave of a patch of several rigid bars, and found that near Bragg resonance the amplitude of the free-surface oscillations at the wall can vary between 1 to 3.6 times the amplitude of the incident waves, depending on the distance between the bars and the wall. It thus appears that

Bragg resonance does not necessarily help protect the shoreline from the incident sea. Kirby & Anton attributed the amplification to possible resonance of the region between the end of the bar patch and the wall.

O'Hare & Davies (1993) studied sand bars under partially reflected waves, experimentally and numerically. While their emphasis was on the evolution of sand bars on an erodible bed, they also gave some numerical results for rigid bars. Two of their computations (in their figure 15) show that when the bar crests were just upwave of the wave envelope *nodes*, the amplitude of the waves decreased shoreward over the patch. When the shoreline condition was adjusted so that the bar crests were just upwave of the wave envelope *antinodes*, then the amplitude of the waves increased shoreward. The explanation given by O'Hare & Davies was that the incident and beach-reflected waves were affected differently by the bars (one is reflected and the other not).†

Imperfect beach absorption was also considered by Benjamin, Boczar-Karakiewicz & Pritchard (1987) in their attempts to make close comparison with the experiments. But the importance of this shore reflection was not fully examined because the beach reflection coefficient was taken to be real.

In this note, we give an analytical study of the effects of the shore reflection on Bragg resonance, with a view to a deeper understanding of the effects of shoreline reflection on the Bragg resonance. We shall show that the qualitative behaviour of the wave amplitudes over the bar patch depends sensitively on the phase difference between the shore reflection and the bars. A transient analysis is also described to elucidate the physics of this sensitive dependence.

## 2. Envelope equations

As in Mei (1985), we consider the plane problem of a normally incident wavetrain approaching from $x \sim -\infty$ and passing over a finite patch of rigid bars. For simplicity the mean water depth $h$ is assumed to be constant, although modification for a sloping beach is in principle possible in the manner of Mei *et al.* (1988). Focusing on the case of near resonance, we assume that the incident wavelength is approximately twice the bar spacing. In a coordinate system where the $x$-axis coincides with the mean sea surface, and the $z$-axis points upward, the bed profile is given by

$$z = \begin{cases} -h + \frac{1}{2}D\mathrm{e}^{-2\mathrm{i}kx} + \frac{1}{2}D^*\mathrm{e}^{2\mathrm{i}kx} & \text{for } 0 < x < L \\ -h & \text{elsewhere,} \end{cases} \tag{2.1}$$

where

$$D = |D|\,\mathrm{e}^{\mathrm{i}\theta_D} \tag{2.2}$$

is the constant complex bar amplitude and $D^*$ its complex conjugate. The width $L$ is much greater than the wavelength so that $kL \gg 1$. For convenience, we shall refer to $x = 0$ as the seaward end and $x = L$ as the shoreward end of the patch. A shoreline or a seawall exists at some distance $x = L + L_f$.

For gentle waves, the leading-order velocity potential is given by

$$\phi = \frac{\mathrm{i}g}{2\omega}\frac{\cosh k(z+h)}{\cosh kh}\left(A\mathrm{e}^{-\mathrm{i}kx} - B\mathrm{e}^{\mathrm{i}kx}\right)\mathrm{e}^{\mathrm{i}\omega t} + \text{c.c.}, \tag{2.3}$$

† They state that if "... the bar crests are upwave of the *antinodes*, the incident wave propagates over the bars without reflection, but the beach reflected wave is re-reflected. As a general rule, waves which encounter a bar crest directly after propagating through an antinode will be reflected" (p. 1173, O'Hare & Davies 1993).

where $\omega$ denotes the wave frequency related to the wavenumber $k$ by

$$\omega^2 = gk \tanh kh. \tag{2.4}$$

The water depth is assumed to be finite, i.e. $kh = O(1)$. The amplitudes of the incident ($A$, right-going) and the reflected ($B$, left-going) waves are known to be governed by the following asymptotic equations (Mei 1985):

$$\frac{\partial A}{\partial t} + C_g \frac{\partial A}{\partial x} = -\frac{\mathrm{i}D\omega k}{2 \sinh 2kh} B, \tag{2.5}$$

$$\frac{\partial B}{\partial t} - C_g \frac{\partial B}{\partial x} = -\frac{\mathrm{i}D^* \omega k}{2 \sinh 2kh} A, \tag{2.6}$$

where

$$C_g = \frac{1}{2}\frac{\omega}{k}\left(1 + \frac{2kh}{\sinh 2kh}\right) \tag{2.7}$$

is the group velocity. Compared respectively to the wave period $2\pi/\omega$ and the wavelength $2\pi/k$, the time and space scales of variations of $A$ and $B$ are much greater by a factor of $1/\epsilon$, where $\epsilon$ is the typical steepness of the waves and the bars, i.e. $\epsilon = O(kA, kB, kD)$.

Over the flat sections of the bed ($x < 0, x > L$), the right-hand sides of (2.5) and (2.6) vanish, so that $A$ and $B$ propagate with the group velocity without changing their values. At the incident end $x = 0$ we require that $A$ equal the prescribed amplitude of the incident wavetrain, i.e.

$$A(0, t) = \text{given}, \quad \text{at } x = 0. \tag{2.8}$$

At the transmission end, $B(L) \neq 0$ due to the presence of the shoreline or seawall at distance $x = L + L_f$. In general, a complex reflection coefficient $B/A$ can be specified at $x = L + L_f$ by empirical knowledge of the shore. At the steady state, this effect of the shoreline can be represented by the complex reflection $R_L$ at $x = L$, i.e.

$$R(L) \equiv R_L = \frac{B}{A} \quad \text{at } x = L. \tag{2.9}$$

For example, if there is a perfectly reflecting vertical wall at $x = L + L_f$ and the incident wavenumber is slightly detuned from perfect resonance by $K$ where $K = \epsilon k \ll k$, then vanishing of the normal velocity at the wall gives

$$R_L = \mathrm{e}^{\mathrm{i}\pi - 2\mathrm{i}[kL + (k+K)L_f]} \tag{2.10}$$

at the steady state. We remark that the boundary condition (2.9) can be equivalently stated for $A$ as

$$\frac{\partial A}{\partial t} + C_g \frac{\partial A}{\partial x} = -\frac{\mathrm{i}D\omega k}{2 \sinh 2kh} R_L A \quad \text{at } x = L. \tag{2.11}$$

From the basic equations (2.5) and (2.6), it can be shown that

$$\frac{\partial}{\partial t}\left(|A|^2 + |B|^2\right) + C_g \frac{\partial}{\partial x}\left(|A|^2 - |B|^2\right) = 0 \tag{2.12}$$

(Mei 1985, equation (2.31)) which states that the rate of the total energy increase at any station is equal to the convergence of the wave energy flux $\frac{1}{2}C_g(|A|^2 - |B|^2)$. In the absence of viscous dissipation, this energy flux must reduce to a constant over the patch at the steady state. It follows that the spatial variation of $|A|^2$ and $|B|^2$ must have the same trend. How each of them varies depends both on the bars and the shore reflection, and is the object of this study.

Also, if the input $A(0,t)$ is either constant or sinusoidal in time from $t=0$ onward, then the steady (or quasi-steady) state solution must be reached at the limit of $t\to\infty$, independently of any initial condition, due to back radiation at $x=0$ and partial absorption at the shore.

In the next section we shall give the solutions for the steady state, followed by a detailed analysis of the implied physics. In § 5, we shall discuss sample numerical solutions to the initial boundary value problem in order to understand better how the final steady state is approached.

## 3. Steady-state response to a detuned incident wave

Following Mei (1985), we assume that on the side $x<0$ the incident wave is slightly detuned from the Bragg resonance frequency by an amount $\Omega$, where $\Omega\ll\omega$, such that

$$A = A_0 e^{i(-Kx+\Omega t)} \quad \text{at } x\leqslant 0. \tag{3.1}$$

Here $\Omega = C_g K$ and $A_0$ is the amplitude of the incoming wave. The solutions to (2.5) and (2.6) with the boundary conditions (2.8) and (2.9) have the following forms at the steady state:

$$\frac{A}{A_0} = \mathscr{A}(x)e^{i\Omega t}, \quad \frac{B}{A_0} = \mathscr{B}(x)e^{i\Omega t}, \qquad 0<x<L, \tag{3.2}$$

where $\mathscr{A}(x)$ and $\mathscr{B}(x)$ are given below for two ranges of detuning frequency relative to the cutoff frequency

$$\Omega_0 = \frac{|D|\,\omega k}{2\sinh(2kh)}. \tag{3.3}$$

### 3.1. *Sub-critical detuning:* $0\leqslant\Omega\leqslant\Omega_0$

As in case (ii) in Mei (1985), we set

$$QC_g = \sqrt{\Omega_0^2-\Omega^2} \tag{3.4}$$

and obtain the following solution:

$$\mathscr{A}(x) = \frac{iQC_g\cosh Q(L-x) - \Omega\sinh Q(L-x) - \Omega_0 R_L e^{i\theta_D}\sinh Q(L-x)}{iQC_g\cosh QL - \Omega\sinh QL - \Omega_0 R_L e^{i\theta_D}\sinh QL}, \tag{3.5}$$

$$\mathscr{B}(x)e^{i\theta_D} = \frac{\left[iQC_g\cosh Q(L-x) + \Omega\sinh Q(L-x)\right]R_L e^{i\theta_D} + \Omega_0\sinh Q(L-x)}{iQC_g\cosh QL - \Omega\sinh QL - \Omega_0 R_L e^{i\theta_D}\sinh QL}. \tag{3.6}$$

There are two special limits. The first is that $\Omega=0$, i.e. the surface waves are perfectly tuned with the bars. Now $QC_g\to\Omega_0$, and (3.5) and (3.6) become

$$\mathscr{A}(x) = \frac{i\cosh(\Omega_0/C_g)(L-x) - R_L e^{i\theta_D}\sinh(\Omega_0/C_g)(L-x)}{i\cosh(\Omega_0/C_g)L - R_L e^{i\theta_D}\sinh(\Omega_0/C_g)L}, \tag{3.7}$$

$$\mathscr{B}(x)e^{i\theta_D} = \frac{i\cosh(\Omega_0/C_g)(L-x)R_L e^{i\theta_D} + \sinh(\Omega_0/C_g)(L-x)}{i\cosh(\Omega_0/C_g)L - R_L e^{i\theta_D}\sinh(\Omega_0/C_g)L}. \tag{3.8}$$

The second limit is that $\Omega=\Omega_0$, i.e. detuning at the cutoff frequency. Now $Q\to 0$, and (3.5) and (3.6) reduce to

$$\mathscr{A}(x) = \frac{1+(i\Omega_0/C_g)(1+R_L e^{i\theta_D})(L-x)}{1+(i\Omega_0/C_g)(1+R_L e^{i\theta_D})L}, \tag{3.9}$$

$$\mathscr{B}(x)e^{i\theta_D} = \frac{-(i\Omega_0/C_g)(1+R_Le^{i\theta_D})(L-x)+R_Le^{i\theta_D}}{1+(i\Omega_0/C_g)(1+R_Le^{i\theta_D})L}. \tag{3.10}$$

### 3.2. *Super-critical detuning: $\Omega > \Omega_0$*

Let

$$PC_g = \sqrt{\Omega^2-\Omega_0^2}, \tag{3.11}$$

where $P$ is the envelope wavenumber. We obtain from (2.5)–(2.9) that

$$\mathscr{A}(x) = \frac{iPC_g\cos P(L-x)-\Omega\sin P(L-x)-\Omega_0R_Le^{i\theta_D}\sin P(L-x)}{iPC_g\cos PL-\Omega\sin PL-\Omega_0R_Le^{i\theta_D}\sin PL}, \tag{3.12}$$

$$\mathscr{B}(x)e^{i\theta_D} = \frac{\left[iPC_g\cos P(L-x)+\Omega\sin P(L-x)\right]R_Le^{i\theta_D}+\Omega_0\sin P(L-x)}{iPC_g\cos PL-\Omega\sin PL-\Omega_0R_Le^{i\theta_D}\sin PL}. \tag{3.13}$$

As in case (i) in Mei (1985), the amplitudes of the surface waves over the bars exhibit spatial oscillations.

## 4. Physical effects of shoreline reflection

### 4.1. *Sub-critical detuning*

Mei (1985) found for $|R_L| = 0$ that the amplitudes of the incident and the reflected waves always decrease monotonically onshore. Here it is convenient to introduce a phase-shifted reflection coefficient

$$\widetilde{R}_L = |R_L|e^{i(\theta_D+\theta_{RL})}, \tag{4.1}$$

where $\theta_{RL}$ denotes the phase of $R_L$. We now show that with $|R_L| \neq 0$ the variation of $|A|$ and $|B|$ over the bar patch has three possible trends, depending on the complex coefficient $\widetilde{R}_L$. As pointed out before, the spatial trends of $|A|$ and $|B|$ across the bar patch are similar due to the constancy of the total energy flux at the steady state, so we need only examine one of them, say $|B|$.

From (3.6), the intensity of the reflected waves over the bar patch is

$$|\mathscr{B}(x)|^2 = \frac{\mathscr{I}(x_1)}{\left|iQC_g\cosh QL-\Omega\sinh QL-\Omega_0R_Le^{i\theta_D}\sinh QL\right|^2}, \tag{4.2}$$

where

$$\mathscr{I}(x) = [\Omega_0^2+2\Omega_0\Omega\,\mathrm{Re}\,(\widetilde{R}_L)]\sinh^2Q(L-x)+\Omega_0^2|R_L|^2\cosh^2Q(L-x) \\ -\Omega_0QC_g\,\mathrm{Im}\,(\widetilde{R}_L)\sinh 2Q(L-x)-\Omega^2|R_L|^2, \tag{4.3}$$

with Re(·) and Im(·) denote, respectively, the real and imaginary parts of the quantity inside the parentheses. To study the spatial variation of $|\mathscr{B}(x)|$, we calculate the first two derivatives of $\mathscr{I}(x)$ with respect to $x$. Denoting

$$c_1 = \Omega_0^2(1+|R_L|^2)+2\Omega_0\Omega\,\mathrm{Re}\,(\widetilde{R}_L), \quad c_2 = 2\Omega_0QC_g\,\mathrm{Im}\,(\widetilde{R}_L), \tag{4.4}$$

we then get from (4.3) that

$$\mathscr{I}_x = -Q\left[c_1\sinh^2 2Q(L-x)-c_2\cosh^2 2Q(L-x)\right], \tag{4.5}$$

$$\mathscr{I}_{xx} = 2Q^2\left[c_1\cosh^2 2Q(L-x)-c_2\sinh^2 2Q(L-x)\right]. \tag{4.6}$$

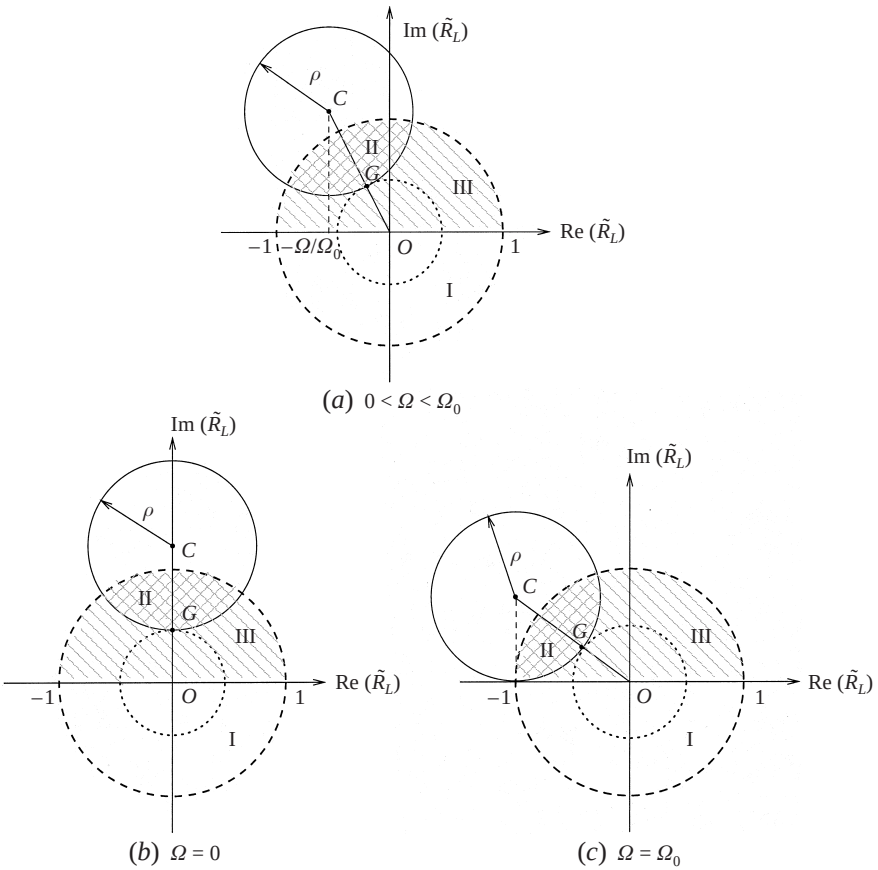


FIGURE 1. Complex plane of $\widetilde{R}_L$ for sub-critical detuning. Region I (semicircle in the lower half-plane): $A$ and $B$ decrease monotonically shoreward. Region II (doubly hatched): $A$ and $B$ increase monotonically shoreward, Region III (singly hatched): $A$ and $B$ first decrease then increase shoreward.

Since from (4.4)

$$c_1 - c_2 = (\Omega_0 \operatorname{Re}(\widetilde{R}_L) + \Omega)^2 + (\Omega_0 \operatorname{Im}(\widetilde{R}_L) - QC_g)^2 > 0$$

and $\cosh y > \sinh y$, it then follows from (4.6) that $\mathscr{I}_{xx} > 0$ everywhere. Hence $\mathscr{I}_x$ increases with $x$. There are three possibilities, corresponding to three regions in the unit circle in the complex plane of $\widetilde{R}_L$.

**Region I:** *Both incident and reflected waves decrease monotonically onshore.* This is the case where the shore is always protected by the bar patch. It occurs when $\mathscr{I}_x \leqslant 0$ at $x = L$, hence $\mathscr{I}_x < 0$ everywhere in $0 < x < L$ and $|\mathscr{B}(x)|^2$ decreases with $x$. From (4.5),

$$\mathscr{I}_x = 2Q\Omega_0 \sqrt{\Omega_0^2 - \Omega^2}\, \operatorname{Im}(\widetilde{R}_L) \quad \text{at } x = L. \tag{4.7}$$

Clearly, $\mathscr{I}_x(L) \leqslant 0$ if and only if

$$\operatorname{Im}(\widetilde{R}_L) \leqslant 0, \tag{4.8}$$

which is the lower half-plane of $\widetilde{R}_L$. Since $|R_L| \leqslant 1$, this region is in fact the lower

half of the unit circle, centred at the origin of the complex plane of $\widetilde{R}_L$, as shown in figure 1(*a–c*).

**Region II:** *Both incident and reflected waves increase monotonically shoreward.* This occurs when $\mathscr{I}_x \geqslant 0$ at $x = 0$, hence $\mathscr{I}_x > 0$ everywhere in $0 < x < L$ and $|\mathscr{B}(x)|^2$ increases with $x$. Upon inserting $c_1$ and $c_2$ and setting $x = 0$, it can be shown from (4.5) that $\mathscr{I}_x(0) \geqslant 0$ when

$$\left(\mathrm{Re}\,(\widetilde{R}_L) + \frac{\Omega}{\Omega_0}\right)^2 + \left(\mathrm{Im}\,(\widetilde{R}_L) - \frac{QC_g}{\Omega_0}\coth 2QL\right)^2 \leqslant \left(\frac{QC_g/\Omega_0}{\sinh 2QL}\right)^2. \tag{4.9}$$

When plotted in the complex plane of $\widetilde{R}_L$, this inequality represents the interior of the circle $\mathscr{C}$ centred at the point

$$C = \left(-\frac{\Omega}{\Omega_0}\,,\ \frac{QC_g}{\Omega_0}\coth 2QL\right) \tag{4.10}$$

with radius

$$CG = \varrho = \frac{QC_g/\Omega_0}{\sinh 2QL}. \tag{4.11}$$

Because of the constraint that $|R_L| \leqslant 1$, only the intersection of $\mathscr{C}$ with the unit circle is of physical relevance, as shown by the doubly hatched area in figure 1(*a*).

The distance between the centre $C$ and the origin $O$ is, from (4.10),

$$OC = \sqrt{\left(\frac{\Omega}{\Omega_0}\right)^2 + \left(\frac{QC_g}{\Omega_0}\coth 2QL\right)^2} = \sqrt{1 + \left(\frac{QC_g/\Omega_0}{\sinh 2QL}\right)^2} > 1. \tag{4.12}$$

Thus the centre of the circle $\mathscr{C}$ is always located outside the unit circle. However, the distance from the origin to the point $G$ where the circle $\mathscr{C}$ intersects the line segment $OC$ is

$$OG = OC - CG = \sqrt{1+\varrho^2} - \varrho = \frac{1}{\sqrt{1+\varrho^2}+\varrho} < 1. \tag{4.13}$$

Therefore the circle $\mathscr{C}$ always intersects the unit circle, implying that the monotonic and exponential increase of $|\mathscr{A}(x)|$ and $|\mathscr{B}(x)|$ onshore is physically feasible when reflection at the shoreward edge is strong and satisfies (4.9). In this case, the bar patch amplifies the wave energy towards the shoreline, and hence may cause strong sediment motion near the shore and pose threats to coastal structures.

In the limit of perfect tuning ($\Omega = 0$), the circle $\mathscr{C}$ and its interior are given from (4.9) by

$$(\mathrm{Re}\,(\widetilde{R}_L))^2 + (\mathrm{Im}\,(\widetilde{R}_L) - \coth 2QL)^2 \leqslant \frac{1}{\sinh^2 2QL} \tag{4.14}$$

and is plotted in figure 1(*b*). In the limit of detuning at the cutoff ($\Omega = \Omega_0$), the inequality (4.9) reduces to

$$(\mathrm{Re}\,(\widetilde{R}_L) + 1)^2 + \left(\mathrm{Im}\,(\widetilde{R}_L) - \frac{C_g}{2\Omega_0 L}\right)^2 \leqslant \left(\frac{C_g}{2\Omega_0 L}\right)^2, \tag{4.15}$$

as shown in figure 1(*c*). In all three cases, the circle $\mathscr{C}$ is always in the upper half-plane of $\widetilde{R}_L$.

**Region III:** *Both incident and reflected waves decrease first then increase onshore.* Referring to figure 1(*a–c*), this case corresponds to the singly hatched area in the upper half of the unit circle. $\mathscr{I}_x = 0$ occurs at $x_m$, where $0 < x_m < L$. To the left of

$x_m$, $\mathscr{I}_x < 0$, hence $\mathscr{I}$ decreases with $x$. To the right $\mathscr{I}_x > 0$, and $\mathscr{I}$ increases with $x$. The limit at which the minimum $\mathscr{I}(x_m)$ occurs at $x_m = L$ is the boundary between Region I and Region III where $\mathrm{Im}(\widetilde{R}_L) = 0$. For perfect tuning, the minimum $\mathscr{I}(x_m)$ is equal to zero, so there is no reflected wave $B$ at this point. The origin of the plane $\widetilde{R}_L$ is the only case studied in Mei (1985).

Let us examine the effects of the total width of the bar patch. As $L$ increases, we see from (4.9), (4.14) and (4.15) that the radius of the circle $\mathscr{C}$ decreases and the centre $C$ moves towards the unit circle, thus Region II diminishes in area. At the limit $L \to \infty$, the circle $\mathscr{C}$ reduces to a single point $C' = (-\Omega/\Omega_0\ , \sqrt{1-(\Omega^2/\Omega_0^2)})$ on the unit circle. Note that the sequence of the two limits $L \to \infty$ and $R_L \to C'$ is important: $\lim_{R_L \to C'} \lim_{L\to\infty} |\mathscr{A}| = 0$ from (3.5), but $\lim_{L\to\infty} \lim_{R_L \to C'} |\mathscr{A}| = \infty$. Setting $L \to \infty$ first means physically that no incident waves can ever reach $L$, hence $R_L$ is practically ineffective. The second limit means that the incident wave is always able to reach the far end at $x = L$ and be reflected there no matter how long the patch is; after waiting long enough the effect of bars at $L$ is always felt.

Sample calculations are shown in figure 2 for $\Omega/\Omega_0 = 0.5$ with three different patch widths ($\Omega_0 L/C_g = 1, 2, 5$). For a fixed phase angle $\theta_D + \theta_{R_L}$, the effects of different reflection coefficients $|R_L|$ are compared. The limiting case $R_L = 0$ in which $|B(x)|$ decreases monotonically in $x$ predicted by Mei (1985) is shown by the solid lines. In figure 2($a$) ($\Omega_0 L/C_g = 1$), each curve corresponds to a point on the line segment $OC$ in the complex plane $\widetilde{R}_L$ shown in figure 1. The inclination of $OC$ is about $\theta_D + \theta_{R_L} \simeq 2\pi/3$. For small enough reflection, as for $|R_L| < 0.6$, the complex $\widetilde{R}_L$ is in Region III and $|B(x)|$ first decreases then increases shoreward. For strong reflection, say $|R_L| > 0.6$, the complex $\widetilde{R}_L$ is now in Region II and $|B(x)|$ increases monotonically shoreward. As the phase angle $\theta_D + \theta_{R_L}$ decreases to $\pi/3$ in figure 2($b$), $\widetilde{R}_L$ is outside the circle $\mathscr{C}$, but still in the upper half-plane; all the curves show first the decrease then the increase with $x$. Finally, in figure 2($c$), $\widetilde{R}_L$ is in the lower half-plane (Region I). $|B(x)|$ decreases monotonically with $x$.

The sensitive dependence of the solutions on the phase angle $(\theta_D + \theta_{R_L})$ is particularly significant since it casts doubt on the practicality of the idea of constructing longshore bars for beach protection. For a fixed bar patch, i.e. fixed $\theta_D$, moving $\widetilde{R}_L$ from one quadrant to the next in the complex plane means changing $\theta_{R_L}$ by less than $\pi/2$. This can be achieved either by moving the reflector at the shoreline by less than one-quarter of the bar wavelength (one-eighth of the water wavelength), or by adding or cutting off one-quarter bar wavelength from the patch. Consider for example a perfectly reflecting vertical wall at $x = L + L_f$. The complex reflection coefficient at $x = L$ at steady state is given by (2.10) with

$$\theta_D + \theta_{R_L} = \theta_D + \pi - 2k(L + L_f) - 2KL_f. \tag{4.16}$$

Clearly, to change $(\theta_D + \theta_{R_L})$ by $\pi/2$, one needs only to change $(L + L_f)$ by $1/8$ of the water wavelength, or $1/4$ of the bar wavelength.

For naturally formed bars, the value $\theta_D$, which gives the position of the bar crest (trough), cannot be chosen *a priori*, like that for rigid bars. It is determined not only by the waves but is also affected by the dominant mode of sediment motion (bedload or suspended load), as remarked by Carter, Liu & Mei (1973) and O'Hare & Davies (1993). Our theoretical study in progress shows that the position of sand bars is a dynamical consequence of the shoreline reflection $R_L$ and it changes during the course of the evolution. These details will be reported elsewhere (Yu & Mei 2000).

To see the effects of patch length $L$, we show in figure 2($d$–$f$, $g$–$i$) the results for

$\Omega_0 L/C_g$ equal to 2 and 5, respectively. Referring to figure 1, the radius of the circle $\mathscr{C}$ is now smaller; there is now a wider range of $\widetilde{R}_L$ falling on the line segment $OC$, for which $|B(x)|$ decreases with increasing $x$ over most of the patch. When $|R_L|$ is close to unity along $OC$ (figure 2*d*, *g*), the amplitudes of the incident and the reflected waves can be more than five times greater than that of the incoming waves from the sea. Note that this amplification is achieved by changing $L$ alone, for any given $L_f$ (including $L_f = 0$).

As mentioned in the introduction, O'Hare & Davies (1993) observed in two numerical examples that the wave amplitudes decrease (increase) shoreward if the bar crests are upwave of the wave envelope nodes (antinodes). We confirm and generalize this result analytically in the Appendix. Specifically when $\widetilde{R}_L$ is in Region II every bar crest is downwave of a node but upwave of the next antinode. But when $\widetilde{R}_L$ is in Region I, every bar crest is downwave of an antinode but upwave of the next node. However our interpretation is that this is the consequence of energy exchange between incident ($A$) and reflected ($B$) waves through the intermediary of the bars, rather than one wavetrain being reflected by the bars and the other not.

### 4.2. *Super-critical detuning*

It is seen from (3.12) and (3.13) that the main feature of super-critical detuning is the spatial oscillation of $\mathscr{A}(x)$ and $\mathscr{B}(x)$ at the period $2\pi/P$. If the bar patch is not long enough ($L \leqslant 2\pi/P$), the oscillation of the incident and the reflected waves is not noticeable.

From (3.13) we have

$$|\mathscr{B}|^2 = a_0 + a_1 \cos 2P(L-x) + a_2 \sin 2P(L-x), \tag{4.17}$$

where

$$a_0 = \frac{1}{\gamma^2}\left[\Omega^2 |R_L|^2 + \frac{\Omega_0^2}{2}(1 - |R_L|^2) + \Omega\Omega_0 \operatorname{Re}(\widetilde{R}_L)\right], \tag{4.18}$$

$$a_1 = \frac{1}{\gamma^2}\left[-\frac{\Omega_0^2}{2}(1 + |R_L|^2) - \Omega\Omega_0 \operatorname{Im}(\widetilde{R}_L)\right], \tag{4.19}$$

$$a_2 = \frac{1}{\gamma^2}[-\Omega_0 \operatorname{Im}(\widetilde{R}_L) P C_g], \tag{4.20}$$

and

$$\gamma^2 = \Omega^2 + \Omega_0^2 |R_L|^2 \sin^2 PL - \Omega_0^2 \cos^2 PL + 2\Omega\Omega_0 \operatorname{Re}(\widetilde{R}_L) \sin^2 PL - \Omega_0 P C_g \operatorname{Im}(\widetilde{R}_L) \sin 2PL. \tag{4.21}$$

The amplitude of the oscillation is given by $\sqrt{a_1^2 + a_2^2}$.

In figure 3, numerical calculations are shown for $\Omega/\Omega_0 = 1.5$. For $\Omega_0 L/C_g = 1$ in figure 3(*a–c*), the bar patch is about half of the oscillation period, therefore the solutions appear to be similar to that of the sub-critical case. For a longer patch, $\Omega_0 L/C_g = 5$ in figure 3(*d–f*), $|B|$, as well as $|A|$, oscillates in $x$. The amplitude of the fluctuation is strongly affected by both the magnitude and the phase of $\widetilde{R}_L$.

## 5. Transient development of Bragg reflection

To see why the steady state is so sensitive to the phase angle, it is revealing to study the transient evolution of Bragg resonance by solving the initial-boundary value

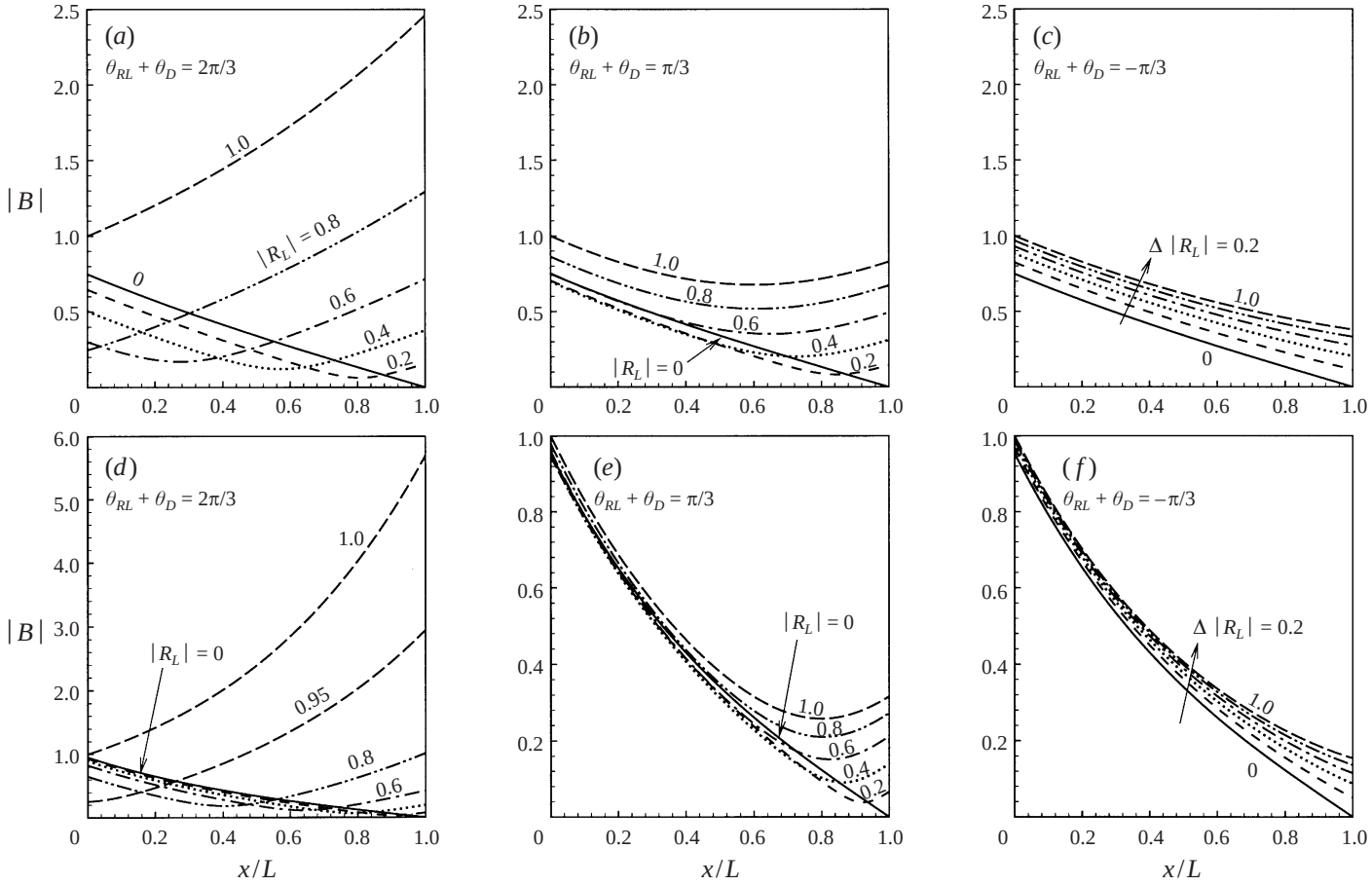


FIGURE 2. For caption see facing page.

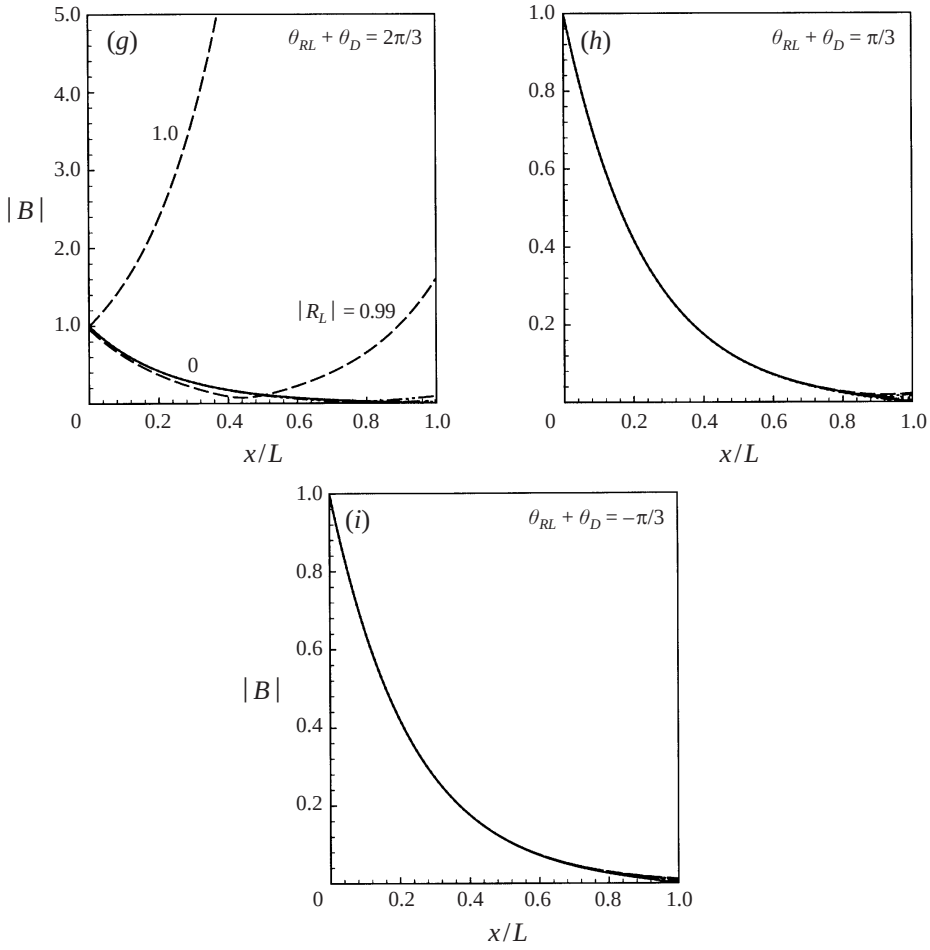


FIGURE 2. Spatial variations of the amplitude of the reflected wavetrain $B$, for sub-critical detuning. ($a$–$c$) $\Omega_0 L/C_g = 1$; ($d$–$f$) $\Omega_0 L/C_g = 2$; ($g$–$i$) $\Omega_0 L/C_g = 5$. $\Omega/\Omega_0 = 0.5$.

problem for (2.5) and (2.6). For convenience, we choose the following normalization:

$$x' = \frac{x}{L}, \qquad t' = \frac{C_g}{L}t, \qquad (A', B') = \frac{(A, B)}{A_0} \tag{5.1}$$

and define

$$\widehat{B}' = -\mathrm{i}B'\mathrm{e}^{\mathrm{i}\theta_D}. \tag{5.2}$$

Then (2.5) and (2.6) become, after dropping primes for brevity,

$$A_t + A_x = \alpha\widehat{B}, \tag{5.3}$$

$$\widehat{B}_t - \widehat{B}_x = -\alpha A, \tag{5.4}$$

for $0 < x < 1$, where

$$\alpha = \frac{\Omega_0 L}{C_g} \tag{5.5}$$

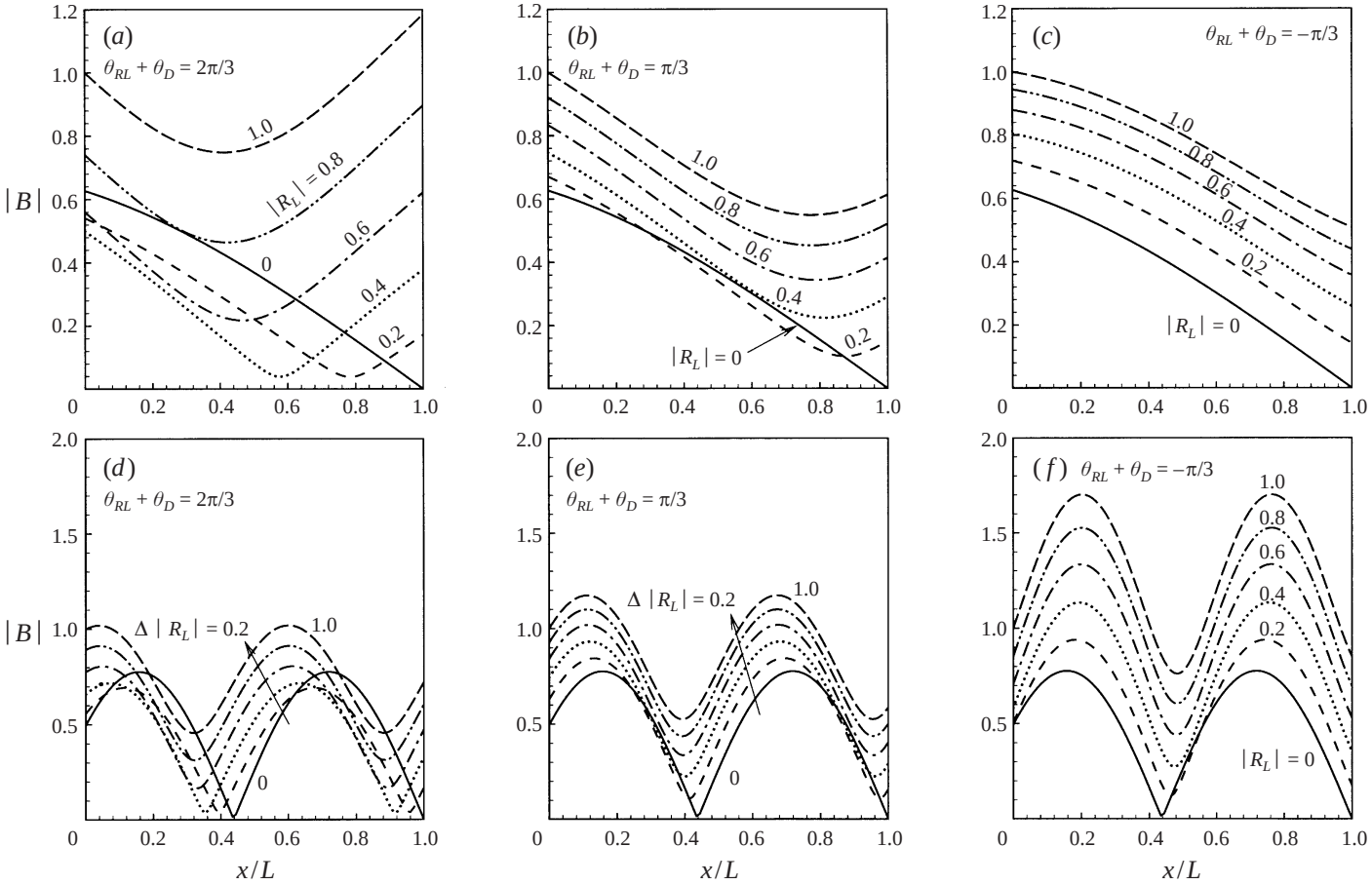


FIGURE 3. Spatial variations of the amplitude of the reflected wavetrain $B$, for super-critical detuning. ($a$–$c$) $\Omega_0 L/C_g = 1$; ($d$–$f$) $\Omega_0 L/C_g = 5$. $\Omega/\Omega_0 = 1.5$.

is real and positive. At the seaward edge,

$$A = \mathrm{e}^{\mathrm{i}(\Omega/\Omega_0)\alpha t} \quad \text{at } x = 0. \tag{5.6}$$

At the shoreward edge of the patch, we assume for simplicity that the bar patch extends all the way up to the shoreline, therefore

$$\frac{\widehat{B}}{A} = -\mathrm{i}\widetilde{R}_L = -\mathrm{i}|R_L|\mathrm{e}^{\mathrm{i}\theta_D + \mathrm{i}\theta_{R_L}} \quad \text{at } x = 1 \tag{5.7}$$

is satisfied during the course of the time evolution. At $t = 0$, the leading edge of the incident wavetrain just arrives at $x = 0$. Thus the initial conditions are

$$A = \widehat{B} = 0 \qquad \text{for } 0 < x \leqslant 1, \quad t = 0. \tag{5.8}$$

Equations (5.3)–(5.8) can readily be solved numerically by a finite difference scheme.† For illustration, we shall consider a perfectly reflecting shore so that $|R_L| = 1$, and perfect tuning ($\Omega = 0$) so that $A(0, t) = 1$. Two special reflection coefficients will be examined:

$$\frac{\widehat{B}}{A} = \pm 1, \quad \text{i.e. } \widetilde{R}_L = \pm\mathrm{i}, \quad \text{at } x = 1. \tag{5.9}$$

It is easy to see that $A(x, t)$ must be real, and so is $\widehat{B}(x, t)$. From (5.3) and (5.4), the equations for energy densities for each wave are

$$\left(\frac{\partial}{\partial t} + \frac{\partial}{\partial x}\right) \tfrac{1}{2}|A|^2 = \alpha\widehat{B}A, \tag{5.10}$$

$$\left(\frac{\partial}{\partial t} - \frac{\partial}{\partial x}\right) \tfrac{1}{2}|\widehat{B}|^2 = -\alpha\widehat{B}A. \tag{5.11}$$

Over the patch of bars there is a transfer of energy between $A$ and $B$. Specifically, if $\widehat{B}A > 0$ is positive, $A$ gains energy from $\widehat{B}$, and hence increases with propagation distance in the $+x$-direction, while $\widehat{B}$ must decrease in amplitude during its propagation in the $-x$-direction.

Results shown in figure 4 correspond to $\widetilde{R}_L = \mathrm{i}$, i.e. $(\widehat{B}/A)_L = 1$, hence to Region II of the complex plane of $\widetilde{R}_L$. On the other hand, results in figure 5 are for $\widetilde{R}_L = -\mathrm{i}$, i.e. $(\widehat{B}/A)_L = -1$, hence Region I. In both sets of figures $A$ and $\widehat{B}$, as well as the shoreward energy flux $\frac{1}{2}(|A|^2 - |B|^2)$, are plotted. For $t < 1$, the results are the same in both cases because the front of the incident wavetrain $A$ has not yet reached the shoreline at $x = 1$; the effect of the shore reflection is not felt. Bragg scattering, already visible at $t = 0.1$, is quite clear by $t = 0.5$. In particular, the reflected wave envelope is being generated behind the right-going front with $\widehat{B} < 0$. Since the energy of $\widehat{B}$ must be transferred from the incident waves, the magnitude of $A$ is reduced except at the entry where $A$ is maintained at the steady input value of unity, and at the front where $\widehat{B} = 0$. Ahead of the front both $A$ and $\widehat{B}$ are zero. This scenario continues up to $t = 1$ when the front of the incident wave envelope reaches the shoreline at $x = 1$. Afterwards the two cases become very different.

$(\widehat{B}/A)_L = 1$: In this case, shore reflection, manifested through $\widetilde{R}_L$, forces a train of reflected waves with phases opposite to those generated by local energy transfer from $A$. As this reflected front propagates back toward $x = 0$ and then beyond to $x < 0$, there is a tendency to reverse the amplitude of $\widehat{B}$ from negative to positive values.

† Analytical solution by, e.g., Laplace transform is in principle possible but unwieldy.

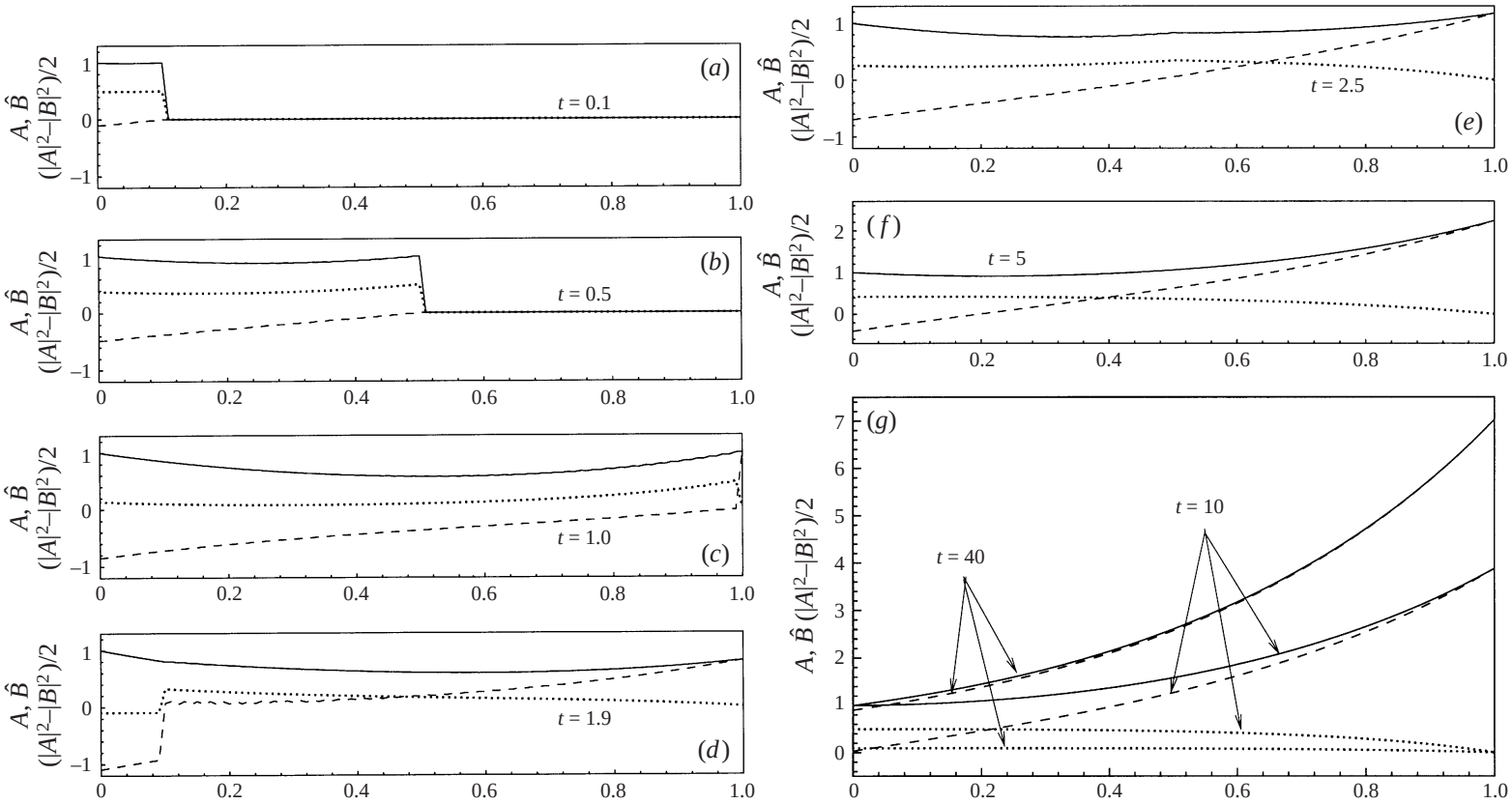


FIGURE 4. Transient evolution for $\widetilde{R}_L = \mathrm{i}$ and $\alpha = 2$. Solid curve: $A$; dashed curve: $\widehat{B}$; dotted curve: $\frac{1}{2}(|A|^2 - |B|^2)$ (energy flux).

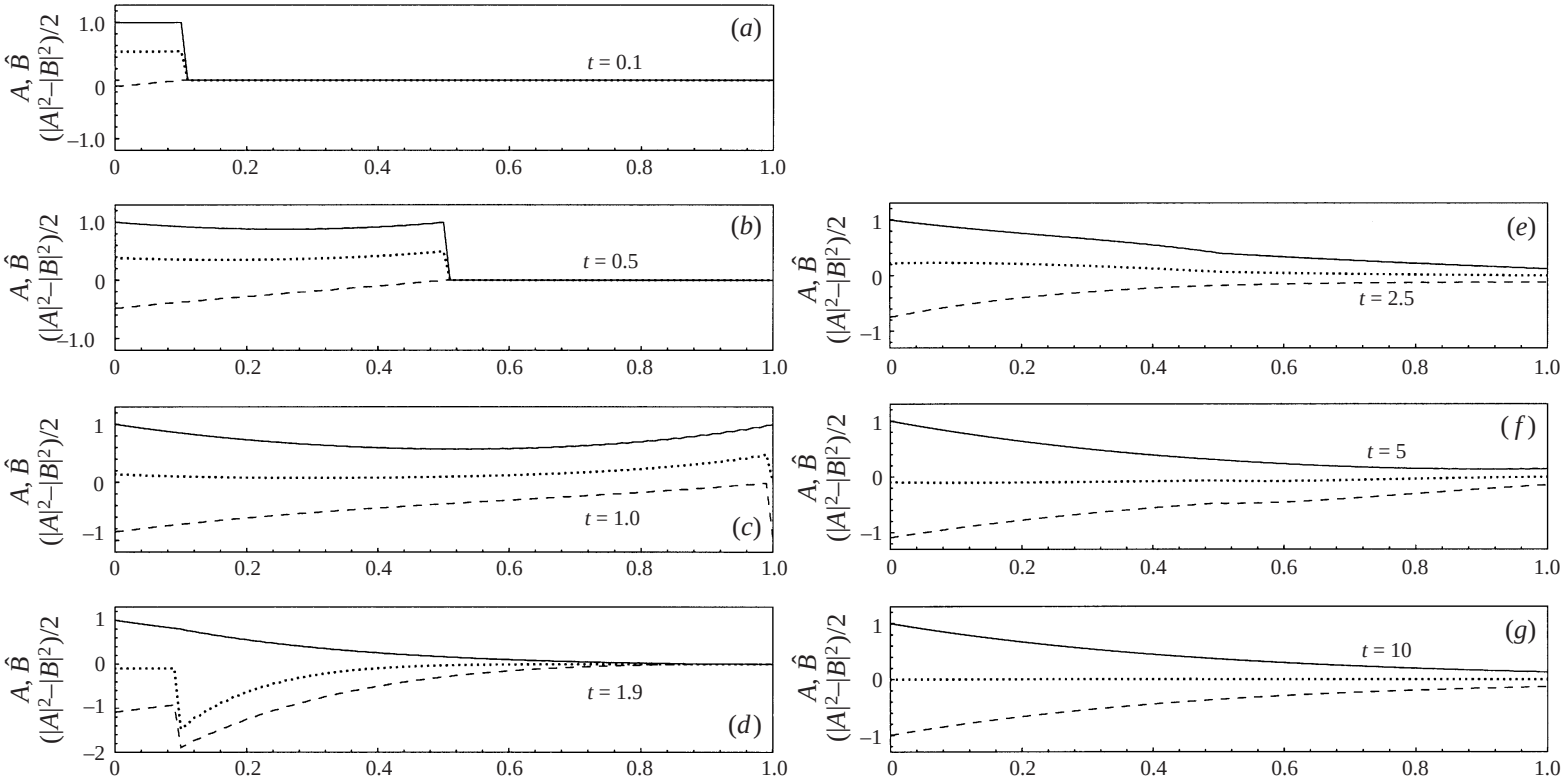


FIGURE 5. Transient evolution for $\widetilde{R}_L = -\mathrm{i}$ and $\alpha = 2$. Solid curve: $A$; dashed curve: $\widehat{B}$; dotted curve: $\frac{1}{2}(|A|^2 - |B|^2)$ (energy flux).

Now to the right of this reflected front where $\widehat{B} > 0$, see figure 4($d$) for $t = 1.9$, $A$ gains energy from $\widehat{B}$ according to (5.10); meanwhile the magnitude of $\widehat{B}$ diminishes in its propagation direction ($-x$) due to energy loss to $A$. As a result, there is a shoreward energy flux to the right of this reflected front. To the left of this front, the effect of shore reflection has not been felt, $\widehat{B} < 0$ and receives energy from $A$. As time goes on, the positive contribution of shore reflection to $\widehat{B}$ gradually wins over the negative contribution of the local scattering, as shown in figure 4($e, f$) for $t = 2.5$, 5.0. Gradually the influence of shore reflection dominates and $\widehat{B}$ becomes positive everywhere, see figure 4($g$) for $t = 10$. Note that in all these figures the energy flux is shoreward, implying the trapping of energy near the shoreward edge. Receiving energy constantly from $\widehat{B}$, $A$ near $x = 1$ has increased markedly. Forced by shore reflection, $\widehat{B}$ has also increased. Finally at $t = 40$ (see figure 4$g$) the state of equilibrium is practically reached, at which $A = \widehat{B} = \mathrm{e}^{\alpha x}$. Now the incident energy from $A$ is exactly carried back to the sea from the patch by the reflected waves. The total energy flux $\frac{1}{2}(|A|^2 - |\widehat{B}|^2)$ is then zero everywhere.

$(\widehat{B}/A)_L = -1$: Here shore reflection sends back reflected waves with the same sign as those generated by local energy transfer from $A$, i.e. $\widehat{B} < 0$, see figure 5($c$) for $t = 1.0$. Because of this the magnitude of $A$ is steadily reduced near the shoreward edge (cf. (5.10)), resulting in turn in the reduction of $\widehat{B}$ at $x = 1$. Near the seaward end $x = 0$, the steady supply of energy from $x < 0$ maintains the level of $A$. These events can be seen in figure 5($d$) for $t = 1.9$. Note the large negative (seaward) energy flux to the right of the reflected front, in contrast to the previous case (cf. figure 4$d$). After $t = 2$, $\widehat{B}(0)$ almost reaches $-1$ so that the energy carried out by $\widehat{B}$ at $x = 0$ nearly balances that brought in by $A$, see figure 5($e, f$) for $t = 2.5$, 5. The equilibrium state ($A = -\widehat{B} = \mathrm{e}^{-\alpha x}$) is approached rather rapidly.

These two examples clearly show how different shore reflection coefficients $R_L$ contribute to the qualitative difference in the final steady states of Bragg resonance.

## 6. Conclusions

The main result of this study is that a patch of rigid bars in front of a beach or seawall can either provide shelter or worsen the hazards of the incident sea, depending on the condition of the shore reflection. As the mechanism is essentially a bar-mediated transfer of energy between incident (right-going) and reflected (left-going) wavetrains, the phase of the shoreline reflection relative to that of bars determines how the energy is transferred locally, and hence is a key to the qualitative change of wave response. In particular, small changes of the location or the total length of the patch can alter this phase relation significantly. Such a sensitive dependence suggests that the potential application of Bragg reflection for beach protection is fraught with uncertainties and is not promising.

We gratefully acknowledge the financial support by US National Science Foundation (Grant CTS directed by Dr Roger Arndt and Dr John Foss), and Office of Naval Research (Grant N00014-92-J-1754, directed by Dr Thomas Swean). We also thank a referee for bringing O'Hare & Davies (1993) to our attention.

## Appendix. Position of bars relative to the wave envelope

From the velocity potential (2.3), the wave envelope nodes (minimum vertical displacement at the free surface) occur at the stations where

$$\cos(2kx + \theta_R) = 1 \quad \text{or} \quad 2kx + \theta_R = 0, 2\pi, \ldots, \tag{A 1}$$

where $\theta_R$ is the phase angle of local reflection coefficient $R = B/A$. The antinodes (maximum vertical displacement at the free surface) occur at

$$\cos(2kx + \theta_R) = -1 \quad \text{or} \quad 2kx + \theta_R = \pi, 3\pi, \ldots . \tag{A 2}$$

From the bottom profile (2.1), the bar crests are located at $2kx - \theta_D = 0, 2\pi, \ldots$ or equivalently,

$$2kx + \theta_R = (\theta_R + \theta_D),\ 2\pi + (\theta_R + \theta_D), \ldots . \tag{A 3}$$

It follows immediately that if $0 < \theta_R + \theta_D < \pi$ the bar crest is downwave of a wave node but upwave of the next antinode; if $\pi < \theta_R + \theta_D < 2\pi$ the crest is downwave of an antinode but upwave of the next node.

For steady state with detuning, (3.2) can be substituted into (2.5) to get the following equation for $|A|$:

$$C_g \frac{\partial |A|}{\partial x} = \Omega_0 |B| \sin(\theta_R + \theta_D). \tag{A 4}$$

Thus, when $\sin(\theta_R + \theta_D) < 0$, i.e. $\pi < \theta_R + \theta_D < 2\pi$, $|A|$ decreases with $x$ (shoreward); when $0 < \theta_R + \theta_D < \pi$, $|A|$ increases with $x$. In view of the analysis in § 4.1, when $\widetilde{R}_L$ is in Region I and waves decrease monotonically shoreward over the patch, each bar crest must be downwave of an antinode and upwave of the next node ($\pi < \theta_R + \theta_D < 2\pi$ everywhere). When $\widetilde{R}_L$ is in Region II and waves increase monotonically shoreward, each bar crest must be downwave of a node and upwave of the next antinode ($0 < \theta_R + \theta_D < \pi$ everywhere). For the cases in Region III, $\sin(\theta_R + \theta_D)$ must change sign somewhere inside the patch.

## REFERENCES


Baillard, J. A., DeVries, J. W. & Kirby, J. T. 1992 Considerations in using Bragg reflection for storm erosion protection. *J. Waterway Port Coastal Ocean Engng* **118**, 62–74.

Baillard, J. A., DeVries, J. W., Kirby J. T. & Guza, R. T. 1990 Bragg reflection breakwater: A new shore protection method? *Proc. 22nd Intl Conf. on Coastal Engineering, Delft*, pp. 757–768.

Benjamin, T. B., Boczar-Karakiewicz, B. & Pritchard, W. G. 1987 Reflection of water waves in a channel with corrugated bed. *J. Fluid Mech.* **185**, 249–274.

Carter, T. G., Liu, P. L.-F. & Mei, C. C. 1973 Mass transport by waves and offshore sand bedforms. *J. Waterways, Harbors & Coastal Engng ASCE* **99**, 165–183.

Dalrymple, R. A. & Kirby, J. T. 1986 Water waves over ripples. *J. Waterway Port Coastal Ocean Engng* **112**, 309–319.

Davies, A. G. & Heathershaw, A. D. 1984 Surface wave propagation over sinusoidally varying topography. *J. Fluid Mech.* **144**, 419–443.

Guazzelli, E., Rey, V. & Belzons, M. 1992 Higher-order Bragg reflection of gravity surface waves by periodic beds. *J. Fluid Mech.* **245**, 301–317.

Hara, T. & Mei, C. C. 1987 Bragg scattering of surface waves by periodic bars: theory and experiment. *J. Fluid Mech.* **178**, 221–241.

Heathershaw, A. D. 1982 Seabed-wave resonance and sand bar growth *Nature* **296**, 343–345.

Kirby, J. T. 1986 A general wave equation for waves over rippled bed *J. Fluid Mech.* **162**, 171–186.

Kirby, J. T. 1989 Propagation of surface waves over undulating bed. *Phys. Fluids* A **1**, 1898-1899.

Kirby, J. T. 1993 A note on Bragg scattering of surface waves by sinusoidal bars *Phys. Fluids* A **5**, 380–386.

Kirby, J. T. & Anton, J. P. 1990 Bragg reflection of waves by artificial bars *Proc. 22nd Intl Conf. on Coastal Engineering, Delft*, pp. 757–768.

Liu, P. L.-F. 1987 Resonant reflection of water waves in a long channel with corrugated boundaries. *J. Fluid Mech.* **179** 371–381.

Mattioli, F. 1990 Resonant reflection of a series of submerged breakwaters. *Il Nuovo Cimento* **13**, 823-833.

Mattioli, F. 1991 Resonant reflection of surface waves by non-sinusoidal bottom undulations. *Appl. Ocean Res.* **13**, 49–53.

Mei, C. C. 1985 Resonant reflection of surface water waves by periodic sandbars *J. Fluid Mech.* **152**, 315–337.

Mei, C. C., Hara, T. & Naciri, M. 1988 Note on Bragg scattering of water waves by parallel bars on the seabed. *J. Fluid Mech.* **186**, 147–162.

Mei, C. C. & Liu, P. L.-F. 1993 Surface waves and coastal dynamics. *Ann. Rev. Fluid Mech.* **25**, 215–240.

O'Hare, T. J. & Davies, A. G. 1993 Sand bar evolution beneath partially-standing waves: laboratory experiments and model simulations. *Continental Shelf Res.* **13**, 1149–1181.

Nayfeh, A. H. & Hawwa, M. A. 1994 Interaction of surface gravity waves on a nonuniformly periodic seabed. *Phys. Fluids* **6**, 209–213.

Rey, V., Guazzelli, E. & Mei, C. C. 1996 Resonant reflection of surface gravity waves by one-dimensional doubly sinusoidal beds. *Phys. Fluids* **8**, 1525–1530.

Yoon, S. B. & Liu, P. L.-F. 1987 Resonant reflection of shallow-water waves due to corrugated boundaries. *J. Fluid Mech.* **180**, 451–469.

Yu, J. & Mei, C. C. 2000 Formation of sand bars under surface waves. *Sub judice.*